Regulatory interactions between two actin nucleators, Spire and Cappuccino

Margot E. Quinlan,[2] Susanne Hilgert,[1] Anaid Bedrossian,[1] R. Dyche Mullins,[2] and Eugen Kerkhoff[1]

[1]Bayerisches Genomforschungsnetzwerk (BayGene), Institut für funktionelle Genomik, Universität Regensburg, 93053 Regensburg, Germany
[2]Department of Cellular and Molecular Pharmacology, University of California, San Francisco, San Francisco, CA 94107

Spire and Cappuccino are actin nucleation factors that are required to establish the polarity of *Drosophila melanogaster* oocytes. Their mutant phenotypes are nearly identical, and the proteins interact biochemically. We find that the interaction between Spire and Cappuccino family proteins is conserved across metazoan phyla and is mediated by binding of the formin homology 2 (FH2) domain from Cappuccino (or its mammalian homologue formin-2) to the kinase noncatalytic C-lobe domain (KIND) from Spire. In vitro, the KIND domain is a monomeric folded domain. Two KIND monomers bind each FH2 dimer with nanomolar affinity and strongly inhibit actin nucleation by the FH2 domain. In contrast, formation of the Spire–Cappuccino complex enhances actin nucleation by Spire. In *Drosophila* oocytes, Spire localizes to the cortex early in oogenesis and disappears around stage 10b, coincident with the onset of cytoplasmic streaming.

Introduction

Developing *Drosophila melanogaster* oocytes use both actin and microtubule cytoskeletal systems to construct and maintain internal landmarks that define the dorsal-ventral and anterior-posterior axes (Theurkauf et al., 1992; Clark et al., 1994; Pokrywka and Stephenson, 1995; Polesello et al., 2002). The *cappuccino* and *spire* genes encode actin filament nucleation factors (Quinlan et al., 2005), and mutation of either gene disrupts localization of the earliest known polarity determinants (Manseau and Schupbach, 1989; Manseau et al., 1996). *spire* and *cappuccino* were originally identified in the same genetic screen (Manseau and Schupbach, 1989), and loss of either results in the premature onset of microtubule-dependent fast cytoplasmic streaming during oogenesis, loss of oocyte polarity, and female sterility (Theurkauf, 1994; Emmons et al., 1995). Rosales-Nieves et al. (2006) demonstrated a genetic interaction between *spire* and *cappuccino* by showing that premature cytoplasmic streaming occurs in flies heterozygous for mutations in both genes. Mutation of *Drosophila* profilin (Chickadee) or addition of the actin-depolymerizing toxin cytochalasin D (Emmons et al., 1995; Manseau et al., 1996) also cause premature fast cytoplasmic streaming. Together, these data suggest that actin polymerization driven by Spire (Spir), Cappuccino

(Capu), and Chickadee suppresses fast cytoplasmic streaming until the appropriate point in oogenesis (Serbus et al., 2005).

Consistent with genetic data, Rosales-Nieves et al. (2006) recently showed that Spir and Capu proteins interact directly. These authors found that the N-terminal region of Spir, which contains the kinase noncatalytic C-lobe domain (KIND) and a cluster of actin-binding WH2 domains (Wiskott-Aldrich syndrome protein homology domain 2), binds to the formin homology 2 (FH2) domain of Capu. Their data suggest that interaction is mediated by direct binding of the WH2 cluster to the FH2 domain. These authors report that the Spir–Capu interaction has no effect on actin nucleation by either protein but that interaction with Spir inhibits FH2-dependent cross-linking of actin filaments and microtubules. Based on these data, Rosales-Nieves et al. (2006) propose a model in which Spir and Capu inhibit premature cytoplasmic streaming by cross-linking microtubules to actin filaments in the oocyte cortex.

Interactions between Spir and Capu have been studied only in *Drosophila*, but there is evidence linking the two proteins in other organisms. In sequenced metazoan genomes, Capu family formins appear only in organisms that also contain Spir family genes (Higgs and Peterson, 2005). Mammals have two copies of each gene. Arthropods, including *Drosophila*, contain at least one *spire* and one *cappuccino* gene, whereas nematodes, such as *Caenorhabditis elegans*, contain neither. Because nematodes diverged from arthropods long after Deuterostomes diverged from Protostomes, it appears that nematodes lost both genes at some point in their evolution. Schumacher et al. (2004) found

Supplemental Material can be found at:
http://www.jcb.org/cgi/content/full/jcb.200706196/DC1

that the patterns of *spir-1* and *formin-2* (*fmn2*) expression are nearly identical in developing and adult mice.

We also note that Spir and Capu homologues are found in a variety of polarized cells, including *Drosophila* and *Xenopus laevis* oocytes (Eg6 or *Xenopus* Spir-2; Le Goff et al., 2006), mammalian eggs (Fmn2; Leader et al., 2002), neurons (Leader and Leder, 2000; Schumacher et al., 2004), and polarized epithelial cells (formin-1; Kobielak et al., 2004). In *Xenopus* oocytes, the mRNA of Spir-2 (Eg6) localizes to the vegetal cytoplasm and marks the posterior end of the developing embryo (Le Goff et al., 2006). Knockout of Fmn2 in the mouse produces a maternal effect phenotype in which females are sterile as a result of mispositioning of the meiotic spindle (Leader et al., 2002).

In this study, we investigate the molecular basis of the interaction between Spir and Capu and how the interaction influences actin nucleation. We find that Spir and Capu interact in vivo as well as in vitro. Similar to Rosales-Nieves et al. (2006), we find that the Spir-WH2 cluster interacts with the Capu-FH2 domain. However, we also find that the Spir-KIND domain binds the Capu-FH2 domain with several orders of magnitude higher affinity than the WH2 cluster. This interaction has three functional consequences: (1) the KIND domain potently inhibits actin nucleation by Capu; (2) interaction between the KIND domain and Capu leads to enhanced actin nucleation by Spir; (3) the KIND domain competes with actin filaments and microtubules for binding to the FH2 domain of Capu. The KIND–FH2 interaction is evolutionarily conserved, as we observe the same results using both *Drosophila* and mammalian Spir and Capu family proteins. The direct interaction of Spir and Capu, the fact that the expression patterns of Spir-1 and Fmn2 exactly overlap in the developing nervous system (Schumacher et al., 2004), and the fact that their evolutionary conservation appears to be linked lead us to speculate that Spir and Capu function as part of a complex whose job is to assemble cytoskeletal landmarks for polarity in many systems.

Results

Spir in oogenesis

We find that full-length Spir is sufficient to rescue the *spire* mutant phenotype. The FlyBase Genome lists four gene products, which are all derived from a single *Drosophila spire* gene: Spir-PA, -PB, -PC, and -PD (GenBank/EMBL/DDBJ accession nos. NM_165323, NM_080115, NM_165325, and NM_165324, respectively). Spir-PA and -PB are ~1,000 amino acids and differ by a 29–amino acid insert. Spir-PD is equivalent to the first 584 amino acids of Spir-PA, whereas Spir-PC is approximately the C-terminal half of Spir-PA. Wellington et al. (1999) detected two distinct bands in Northern blots of RNA from fly oocytes, which they named Spire long form and short form (GenBank/EMBL/DDBJ accession nos. AF184975 and AF184976). These correspond to Spir-PA/PB and Spir-PD, respectively. There is no published evidence for the expression of Spir-PC. We made transgenic flies that express monomeric RFP (mRFP)–tagged full-length Spir (we refer to PA/PB as full length) in the germline. The localization of Spir fusions was enriched in the oocyte cortex and diffuse in the oocyte cytoplasm (Fig. S1 A, available

at http://www.jcb.org/cgi/content/full/jcb.200706196/DC1). Rosales-Nieves et al. (2006) expressed GFP fusions of two putative spliceoforms of Spir (GFP-SpirC and GFP-SpirD) in *Drosophila* egg chambers. Consistent with our observation, they found both proteins associated with the oocyte cortex. They also observed GFP-SpirC in punctae and GFP-SpirD diffuse throughout the oocyte. *spir*[1] flies are putative nulls with the stereotypical *spire* phenotypes, including female sterility. Both mRFP-Spir and Spir-mRFP rescue female sterility in *spir*[1] flies, demonstrating that the full-length transcript is sufficient during oogenesis and that the shorter spliceoforms are not essential.

We next determined the localization of endogenous Spir in wild-type *Drosophila* egg chambers by immunofluorescence microscopy (Fig. 1). To distinguish specific from nonspecific staining, we compared wild-type egg chambers with those of homozygous *spir*[1] mutants (Fig. S1, B and C). From early oogenesis through stage 9, Spir localizes specifically to the actin-rich cortex of the oocyte (Fig. 1, A and B). We cannot confirm the diffuse cytoplasmic localization observed in mRFP-Spir flies with immunofluorescence because we also observe it in *spir*[1] flies (Fig. S1 B). At stage 10, near the onset of cytoplasmic streaming, Spir staining disappears from the cortex (Fig. 1 C). Because the loss of Spir produces precocious cytoplasmic streaming, this result suggests that cytoplasmic streaming is normally triggered by the destruction or displacement of Spir from the oocyte cortex.

Spir and Capu interact in vivo

Spir and Capu have been shown to interact in vitro (Rosales-Nieves et al., 2006). To determine whether these proteins interact in vivo, we immunoprecipitated Capu from wild-type *Drosophila* ovary lysates and probed the precipitated material with anti-Spir antibodies. Spir coimmunoprecipitates with Capu but not with beads alone or beads with nonspecific IgG, indicating that Spir and Capu are part of a protein complex in vivo (Figs. 1 D and S1 E).

To further examine the in vivo interaction between Spir and Capu, we studied their subcellular localizations when expressed individually or together in NIH 3T3 fibroblasts. We compared *Drosophila* and mammalian Spir and Capu family proteins and used truncation mutants to map domains required for interaction. As we reported previously, full-length Spir localizes to punctae (Fig. 2 B) that correspond to the trans-Golgi network, post-Golgi vesicles, and recycling endosomes (Kerkhoff et al., 2001). Full-length Capu (myc tagged) is distributed uniformly throughout the cytoplasm (Fig. 2 B). Coexpression of Spir together with Capu induces a striking change in Capu localization. Capu shifts from a diffuse distribution to discrete punctae that coincide with the localization of Spir (Fig. 2 C). Using truncation mutants, we found that the N-terminal portion of Spir and the C-terminal portion of Capu are necessary for colocalization (Fig. S2 B, available at http://www.jcb.org/cgi/content/full/jcb.200706196/DC1). We then coimmunoprecipitated EGFP-Capu-FH2 with myc-Spir-NT from cells expressing both constructs, demonstrating that colocalization corresponds with interaction (Fig. 2 F).

The N-terminal half of the Spir proteins, which is necessary for the colocalization of Spir and Capu, contains two different structural motifs: one KIND domain and a cluster of four
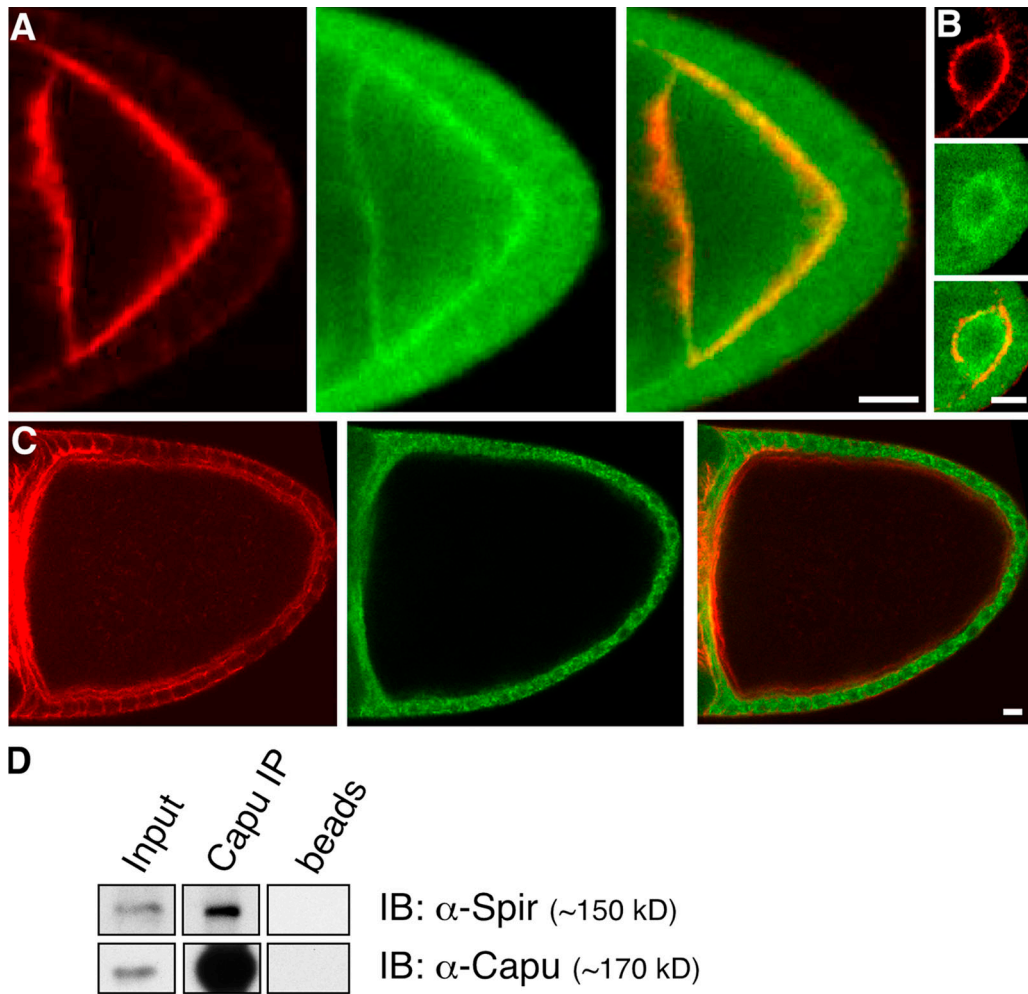
Figure 1. **Localization of Spir in *Drosophila* oocytes.** (A–C) Ovaries were dissected from wild-type flies and processed according to Robinson and Cooley (1997). Spir is detected at the actin-rich oocyte cortex during midoogenesis (green, anti-Spir; red, actin detected with rhodamine-phalloidin). Examples of stage 9 (A) and stage 6 (B) oocytes are shown. Posterior is to the right. For comparison with *spir¹* flies, see Fig. S1. (C) Spir is no longer at the cortex by stage 10b. (D) Spir and Capu interact in vivo. Spir coimmunoprecipitates with Capu from *Drosophila* ovary lysates. 1% of input is shown. Spir did not precipitate with beads alone or beads bound to nonspecific IgG (not depicted). The three boxes in each row are from the same exposure, moved for presentation. For more information, see Fig. S1 (available at http://www.jcb.org/cgi/content/full/jcb.200706196/DC1). Bars, 10 μm.

WH2 domains (Fig. 2 A). Rosales-Nieves et al. (2006) mapped the interaction between Spir and Capu to the Capu-FH2 domain and the Spir-WH2 cluster. They also reported a weak interaction with the ~150–amino acid region adjacent to the WH2 cluster containing the C-terminal half of the KIND domain. However, they did not test for an interaction with the intact KIND domain. We found that the KIND domain is sufficient for colocalization with an EGFP-tagged Capu-FH2 (Fig. 2). We targeted the KIND domain to membranes using a C-terminal Ha-Ras-CAAX motif (Schaber et al., 1990). When expressed in NIH 3T3 fibroblasts, KIND-CAAX localizes to the plasma membrane and to cytoplasmic spots (Fig. 2 D, red). Coexpression of an EGFP-Capu-FH2 led to colocalization with the membrane-targeted KIND (Fig. 2 D). We could not test the WH2 domain in this context because the CAAX motif did not effectively drive WH2 localization to the plasma membrane or distinct punctae (unpublished data).

We also observed the colocalization of mammalian Spir and Capu family proteins (Spir-1 and Fmn2; Fig. S2 C).

The Spir-1–KIND and Fmn2-FH2 domains were sufficient to mediate this interaction (Figs. 2 E and S2 C). The interaction is specific because a KIND domain from the protein very-KIND (VKIND-KIND-CAAX; Mees et al., 2005) does not colocalize with or pull down Fmn2-FH2, nor does the FH2 domain of the formin mDia1 (mDia1-FH2) colocalize with or pull down Spir-1–KIND (Fig. S2, D and E). These data suggest that the interaction between Spir and Capu family proteins is specific and conserved.

Spir and Capu interact directly

To further examine the interaction between Spir and Capu, we determined the affinity of purified KIND for purified Capu-FH1FH2 using fluorescence polarization anisotropy. Capu-FH2 and Capu-FH1FH2 behave similarly, but the longer construct is more stable, so for the majority of experiments, we used Capu-FH1FH2. We labeled an endogenous cysteine in KIND with AlexaFluor488 and measured changes in polarization anisotropy induced by Capu-FH1FH2. We determined the affinity by fitting the data with a quadratic binding curve ($K_d = 1 \pm 2$ nM; Fig. 3 A).
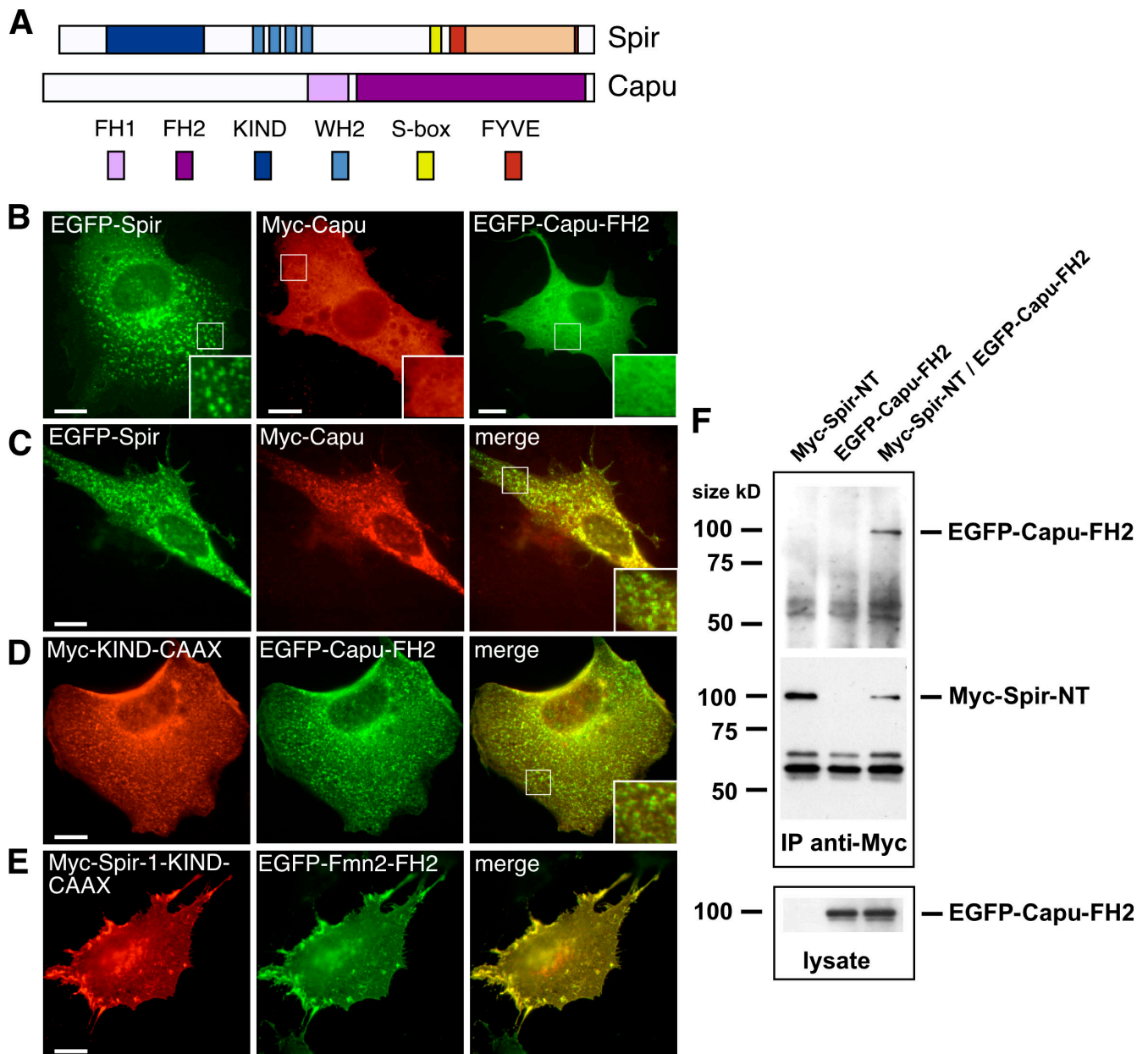
Figure 2. **Interaction of Spir and Capu is mediated by the KIND and FH2 domains.** (A) Domain organization of Spir and Capu. (top) The central region of Spir proteins contains a cluster of four actin-binding WH2 motifs, which nucleate actin. The C-terminal part consists of a modified FYVE zinc finger (mFYVE), which targets the protein to intracellular membranes. The adjacent Spir box (S-box) is similar to motifs found in proteins that bind Rab-3a and may also play a role in subcellular localization. The KIND domain is a novel motif that may function as a protein–protein interaction module. (bottom) Capu, a formin, contains a proline-rich region, the formin homology 1 domain (FH1), and a C-terminal formin homology 2 domain (FH2) that dimerizes and nucleates actin. (B–E) NIH 3T3 cells transfected with individual expression vectors (B) or cotransfected with two expression vectors (C–E) encoding the indicated proteins. EGFP fusion proteins are green, and the myc-tagged counterpart is localized by immunofluorescence using anti-myc antibodies (red). (B) When expressed alone, full-length Capu and Capu-FH2 are diffuse throughout the cell. Spir is punctate as previously described (Kerkhoff et al., 2001). (C) When cotransfected with Spir, the localization of Capu shifts to a punctate pattern coinciding with Spir. (D) The Spir-KIND domain and Capu-FH2 domain are sufficient for colocalization. The KIND domain is driven to membranes by a CAAX box. Capu-FH2 is found concentrated at these same structures. (E) These interactions are conserved in mammalian proteins. Here, we show the colocalization of Spir-1–KIND and Fmn2-FH2 (Fig. S2 C, available at http://www.jcb.org/cgi/content/full/jcb.200706196/DC1). Insets are magnified (2.3 times) images of the boxed areas. (F) Coimmunoprecipitation of EGFP-Capu-FH2 and myc-Spir-NT from NIH 3T3 cells expressing these constructs with a myc antibody. Bars, 10 μm.

To determine whether the label affected binding, we also determined the affinity of unlabeled KIND by using it to compete with the labeled protein ($K_{d2} = 5 \pm 3$ nM; Fig. 3 A, inset). The agreement indicates that attachment of the fluorophore has little effect on the interaction. The affinity measured using

Capu-FH2 rather than FH1FH2 was nearly indistinguishable ($K_d = 9 \pm 6$ nM; Fig. S2 F).

We found that the WH2 cluster binds weakly to Capu-FH1FH2. The addition of Capu-FH1FH2 to AlexaFlour488-labeled WH2 produced a saturable change in fluorescence intensity,
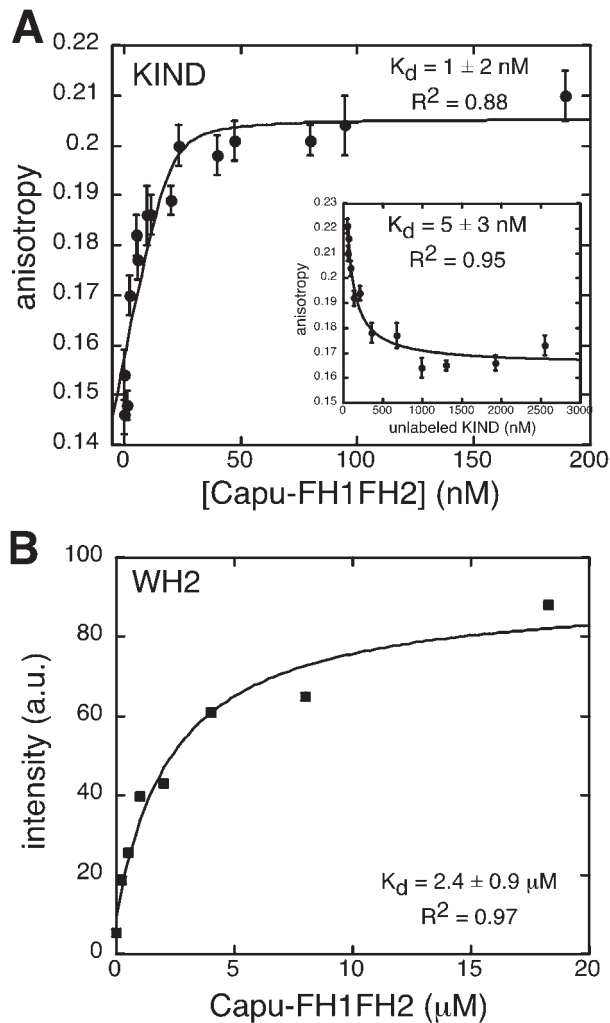
A

KIND

$K_d = 1 \pm 2$ nM
$R^2 = 0.88$

(inset) $K_d = 5 \pm 3$ nM
$R^2 = 0.95$

unlabeled KIND (nM)

anisotropy vs [Capu-FH1FH2] (nM)

B

WH2

$K_d = 2.4 \pm 0.9$ µM
$R^2 = 0.97$

intensity (a.u.) vs Capu-FH1FH2 (µM)

Figure 3. **Binding affinities of direct interactions between Spir and Capu.** (A) Polarization anisotropy of 10 nM AlexaFluor488-labeled KIND in the presence of the Capu-FH1FH2 domain. By fitting the concentration-dependent change in anisotropy to a quadratic binding curve, we determined a dissociation equilibrium constant of 1 ± 2 nM. (inset) Competition of fluorescently labeled KIND with unlabeled KIND. We mixed 10 nM AlexaFluor488-labeled KIND and 50 nM Capu-FH1FH2 with varying concentrations of unlabeled KIND. Fitting the decrease in anisotropy to a competition binding curve (see Materials and methods) yields a dissociation equilibrium constant of 5 ± 3 nM. Error bars represent SD. (B) The affinity of 20 nM AlexaFluor488-labeled WH2 was measured by fitting a quadratic binding curve to concentration-dependent intensity changes induced by adding Capu-FH1FH2. The K_d is 2.4 ± 0.9 µM. Error bars are smaller than the symbols.

so we used fluorescence intensity as a metric for binding. We determined an affinity of 2.4 ± 0.9 µM (Fig. 3 B), which is roughly three orders of magnitude weaker than the affinity of KIND for Capu-FH2. We could not measure the affinity of unlabeled WH2 by competition because higher concentrations of the WH2 domain produced dose-dependent light scattering. This probably reflects aggregation caused by the highly charged WH2 cluster.

We found that the stoichiometry of the KIND–FH2 complex is 2:2 (two KIND monomers/one FH2 dimer). Using velocity sedimentation and equilibrium centrifugation, we first determined that the KIND domains from human Spir-1 and *Drosophila* Spir are both monomeric and highly asymmetric (Fig. 4, A–C).

To measure the stoichiometry of the complex, we combined AlexaFluor488-labeled Capu-FH1FH2 with KIND at three different ratios and spun the mixtures to equilibrium at multiple speeds. We determined the equilibrium distribution of Capu-FH1FH2 by measuring the absorbance of the attached fluorophore. These data were best fit by a single-species model with a molecular mass close to that predicted for two KIND domains plus one Capu-FH1FH2 dimer (predicted, 223.6 kD vs. measured, 225 kD; Fig. 4 D). The fact that the data fit a single-species model is consistent with a high affinity interaction between KIND and Capu-FH1FH2. We detected no evidence of the Capu-FH1FH2 dimer either free or bound to a single KIND domain.

Functional consequences of the Spir–Capu interaction

Spir family proteins inhibit actin nucleation by Capu family formins (Fig. 5 and Fig. S3, available at http://www.jcb.org/cgi/content/full/jcb.200706196/DC1). Because Spir binds the nucleation domain of Capu, we used pyrene-actin fluorescence assays to determine the effect on Capu activity. Both Capu-FH2 and Capu-FH1FH2 promote rapid actin filament assembly. The addition of KIND caused a dose-dependent decrease in nucleation activity (Figs. 5 A and S3 A). Because of local concentration effects, the addition of a weak interaction to a stronger one can have an effect on overall affinity. Thus, we also tested a mutant form of NTSpir (NTSpir[A*B*C*D*] from Quinlan et al., 2005), which includes both the KIND domain and the WH2 cluster but nucleates only very weakly (Fig. S3 B). By plotting the rate of nucleation versus the concentration of KIND (Figs. 5 B and S3 D) and fitting the data with a quadratic binding curve, we determined inhibition constants (K_i). In all cases, Spir inhibited FH2-dependent nucleation by >90% and with comparable apparent affinities (5–10 nM; Fig. 5 B). These K_is agree well with the K_d measured by polarization anisotropy, but, from our data, we cannot determine whether the binding of one or two KIND domains is required for inhibition. We observe the same effect with the mammalian proteins (Fig. S3 C). The K_d and K_i of the Spir-1–KIND–Fmn2-FH2 interaction are higher than observed with *Drosophila* isoforms but, in general, agree with each other (300 ± 60 and 190 ± 40 nM; Figs. S2 G and S3 E).

Neither *Drosophila* nor mammalian KIND affects spontaneous actin assembly (Fig. S4, A and B; available at http://www.jcb.org/cgi/content/full/jcb.200706196/DC1), demonstrating that the effect is specific to the activity of the Capu-FH2 domain. Also, Spir-1–KIND had no effect on actin nucleation by FH2 domains from Diaphanous family formins mDia1 and mDia2 (Fig. S4 C), indicating that the inhibitory effect of Spir-KIND domains is specific to Capu family formins.

Capu does not inhibit actin nucleation by Spir (Fig. 5 C). To assess the effect of Capu on Spir-dependent nucleation, we mutated Capu-FH1FH2. Mutating Ile-706 to Ala (analogous to Ile-1431-Ala in *Saccharomyces cerevisiae* Bni1; Xu et al., 2004) almost completely abolishes nucleation activity. The addition of Capu-FH1FH2(I706A) to NTSpir enhanced nucleation activity (Fig. 5 C, green vs. blue traces). The effect increased with increasing concentrations of Capu-FH1FH2(I706A) until approximately equimolar concentrations of proteins were present.
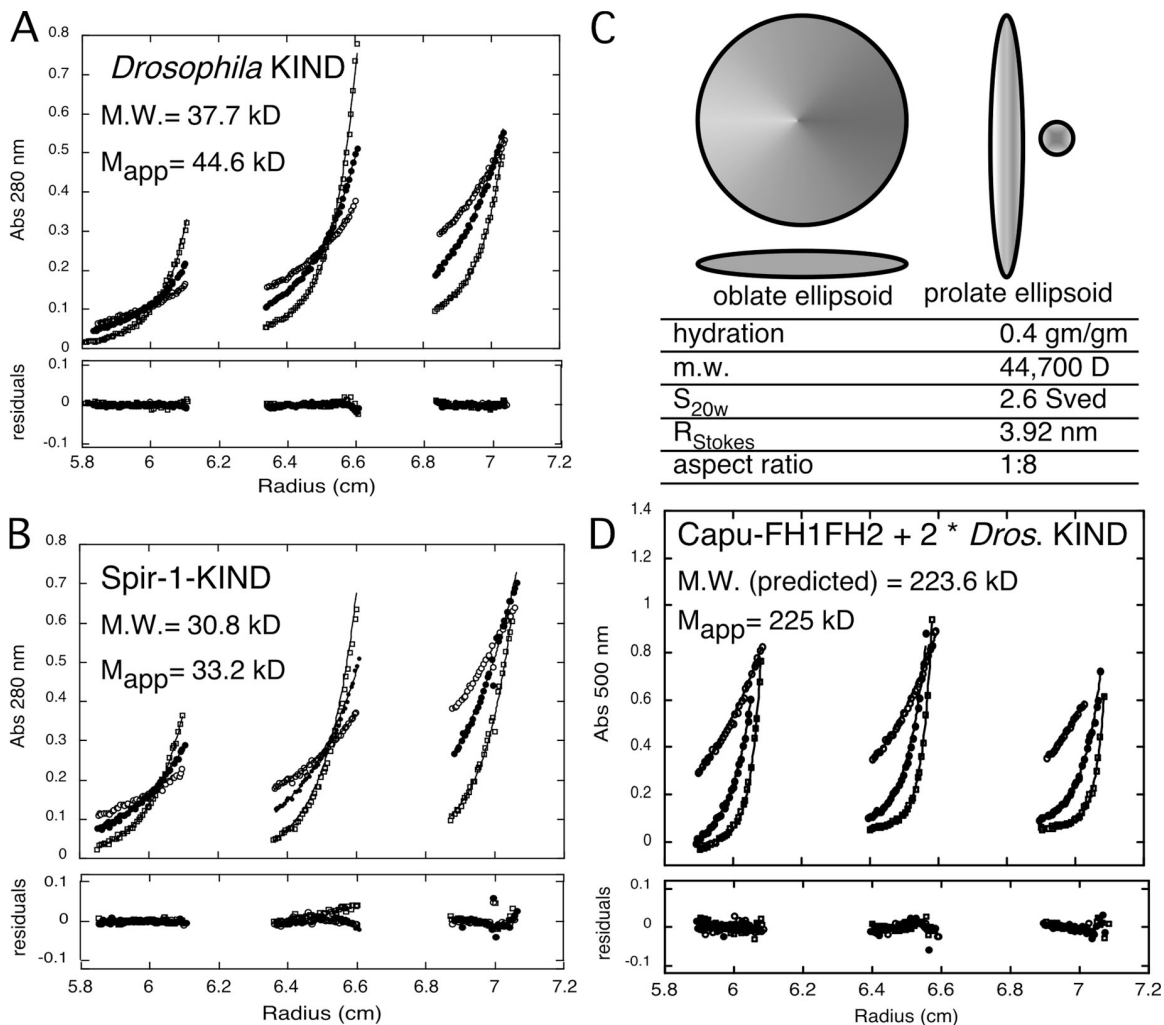
hydration	0.4 gm/gm
m.w.	44,700 D
S_{20w}	2.6 Sved
R_{Stokes}	3.92 nm
aspect ratio	1:8

Figure 4. **Two KIND domains bind each Capu dimer.** (A and B) We determined that KIND domains from *Drosophila* Spir and human Spir-1 are monomeric using equilibrium centrifugation. We measured the solution molecular weights of purified KIND (A) and Spir-1–KIND (B) as described in Materials and methods. We spun samples to equilibrium at 10,000 (open circles), 14,000 (closed circles), and 20,000 rpm (open squares). Symbols are data points; lines represent the best fit to a single species model. Residuals for each dataset are shown below. In both cases, the apparent molecular weight by centrifugation was slightly higher than the predicted monomer molecular weight, suggesting a possible weak tendency to self-associate. By fitting the ultracentrifugation data with a monomer-dimer equilibrium model, we placed lower bounds on the dissociation equilibrium constants for dimerization. For KIND, the K_d for dimerization is at least 92 μM, and, for Spir-1–KIND, it is >530 μM. Neither dataset was well fit by a single-species model with the molecular weight of a KIND homodimer. (C) The KIND domain is highly asymmetric. We measured the sedimentation coefficient, Stokes radius, and aspect ratio of KIND by velocity sedimentation. Both oblate and prolate ellipsoids with an aspect ratio of 1:8 fit the data. The molecular weight measurement agrees with that found by equilibrium sedimentation (44.7 vs. 44.6 kD). Because this value is larger than expected, we confirmed that the actual molecular mass is 37.7 kD with mass spectometry. Velocity sedimentation analysis of Spir-1–KIND indicates a 1:8 aspect ratio as well (not depicted). (D) We measured the solution molecular weight of three molar ratios of AlexaFluor488-labeled Capu-FH1FH2 and KIND (1 [Capu dimer]:1 [KIND], 1:2, and 1:4). We spun samples to equilibrium at 5,000 (open circles), 7,000 (closed circles), and 14,000 rpm (open squares) and measured protein concentration as a function of radius by absorbance at 500 nm to track the AlexaFluor488-labeled protein. The apparent molecular mass of the single species is 225 kD, which is very close to the predicted mass of 223.6 kD (the sum of one Capu-FH1FH2 dimer [134 kD] plus two KIND molecules [M_{app} = 2 × 44.6 kD]). We found that Capu-FH1FH2 alone is unstable under the same conditions (not depicted). Therefore, in the case in which there was excess Capu-FH1FH2 (1:1), we believe that unbound Capu-FH1FH2 precipitated, leaving only the complex to be detected. Conditions: buffer, 50 mM KCl, 10 mM Hepes, pH 7, 1 mM TCEP, and 0.01% sodium azide; temperature, 24°C.

Further increases in Capu-FH1FH2(I706A) concentration decreased activity. This dose response is consistent with an enhancement mechanism dependent on the dimerization of Spir via the KIND–FH2 interaction. We observed the same effect with mammalian isoforms (unpublished data). Although we detect binding between the two domains, the Capu-FH1FH2 domain has no effect on actin nucleation by the WH2 cluster alone (Fig. 5 C, inset), confirming that enhancement depends on interaction between the KIND and FH2 domains.

When active Capu-FH1FH2 and NTSpir are combined, the measured nucleation rate reflects a combination of inhibition and enhancement activity (Fig. 5 D). For example, the rate of polymerization in the presence of 100 nM Capu-FH1FH2 and 250 nM NTSpir falls between the rates of either nucleator alone. Nucleation by 100 nM Capu-FH1FH2 has virtually no lag, whereas nucleation by 250 nM NTSpir has a marked lag (∼30 s). When the two are combined, a long lag is observed that is consistent with the potent inhibition of Capu-FH1FH2 nucleation
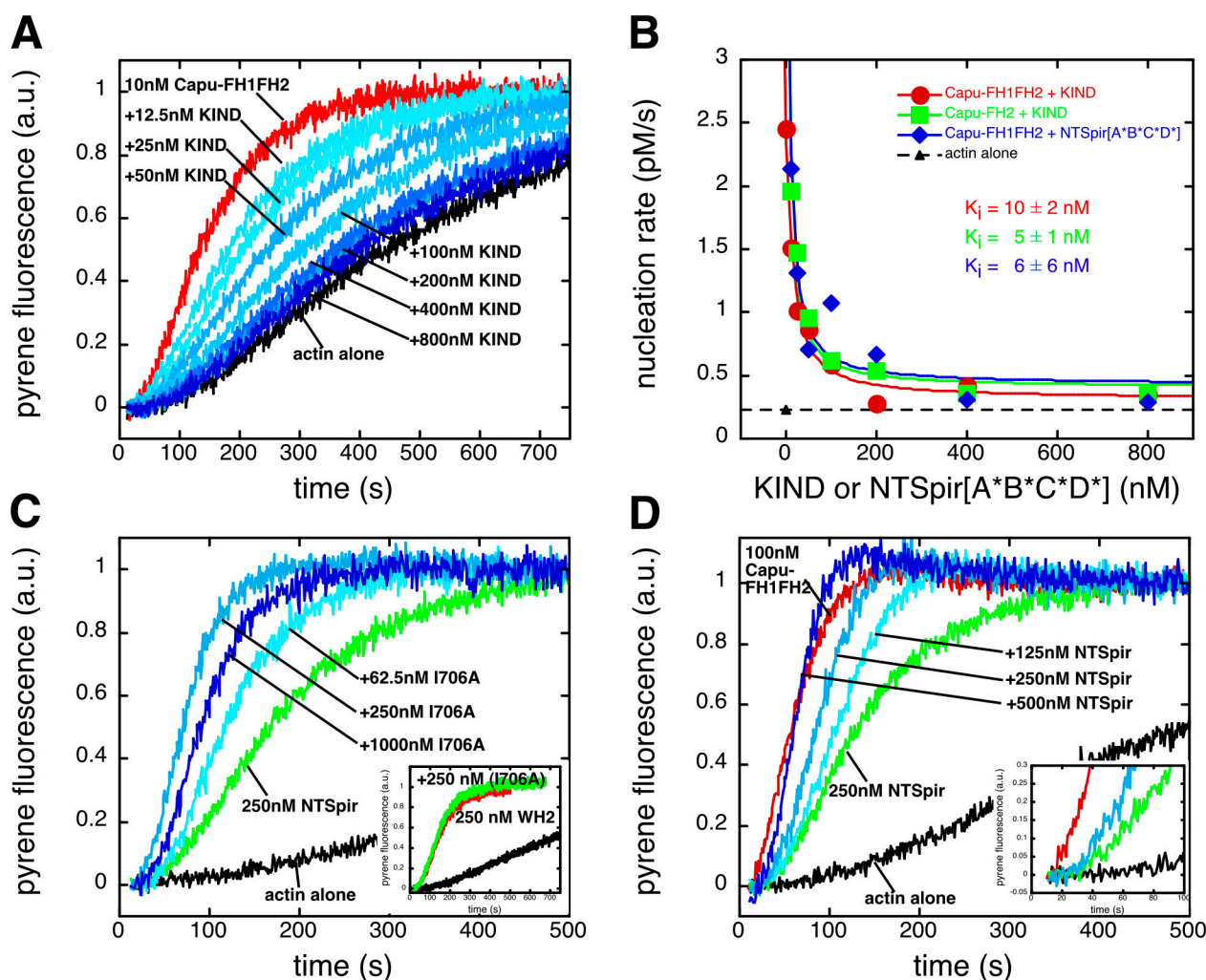
Figure 5. **Interaction between Spir and Capu affects actin nucleation.** (A) The Spir-KIND domain inhibits actin nucleation by Capu family formins. We induced polymerization by mixing pyrene-labeled actin with Mg^{2+}, K^+, and Capu-FH1FH2. The addition of KIND to Capu-FH1FH2 before mixing with actin potently inhibited nucleation activity in a dose-dependent manner. Protein concentrations were as follows: actin, 4 μM (5% pyrene labeled); Capu-FH1FH2, 10 nM; KIND, as indicated. (B) Plot of nucleation rates (calculation shown in Fig. S3 D, available at http://www.jcb.org/cgi/content/full/jcb.200706196/DC1) versus concentration of KIND added. Data were fit with a quadratic binding curve. The inhibition constants for Capu-FH2 ($K_i = 5 \pm 1$ nM), Capu-FH1FH2 ($K_i = 10 \pm 2$ nM), and NTSpir[A*B*C*D*] ($K_i = 6 \pm 6$ nM) are similar, indicating that the effect of KIND is independent of the Capu-FH1 domain and Spir-WH2 cluster. (C) Capu enhances actin nucleation by Spir. We mixed several concentrations of a nucleation-incompetent mutant of Capu-FH1FH2 (Capu-FH1FH2(I706A)) with the N-terminal half of Spir (NTSpir), which contains the KIND domain and four WH2 domains (only three concentrations are shown for clarity). Nucleation activity of NTSpir was increased by Capu-FH1FH2(I706A) until the proteins were approximately equimolar, and then activity decreased. (inset) Capu-FH1FH2(I706A) does not enhance the activity of the WH2 cluster alone, indicating that an interaction between the KIND domain and the formin is necessary. Protein concentrations were as follows: actin, 4 μM (5% pyrene labeled), NTSpir and WH2, 250 nM; Capu-FH1FH2(I706A), as indicated. (D) Capu and Spir affect each other's actin-nucleation activity. 100 nM Capu-FH1FH2 was mixed with a range of NTSpir concentrations. The activity is not the sum of the individual components. Baseline activities are shown for comparison: 100 nM Capu-FH1FH2 (red) and 250 nM NTSpir (green). (inset) Expanded view of the early time shows a lag when Spir and Capu are mixed that is absent for Capu alone.

(Fig. 4 D, inset). Rosales-Nieves et al. (2006) did not observe such synthetic activity when they combined Capu-FH2 and SpirD (equivalent to NTSpir). One possible explanation is that the KIND domain was not folded correctly in these experiments. When we treat NTSpir with denaturant (e.g., GnHCl) or the KIND domain is absent (WH2 alone), Spir retains nucleation activity, but Spir and Capu do not interact in the polymerization assay (Fig. 5 C, inset; and not depicted).

Spir-KIND competes with microtubules for binding to Capu-FH2 (Fig. 6; Rosales-Nieves et al., 2006). The FH2 domain of formins is known to bind microtubules in vitro and in vivo (Wallar and Alberts, 2003). Rosales-Nieves et al. (2006) reported

that Capu-FH2 cross-links actin and microtubules and that this activity is modulated by Spir. We also assessed the ability of Capu family formins to bind microtubules and tested the effect of the KIND domain on this interaction. We found that both *Drosophila* Capu and Fmn2 cosediment with microtubules (Fig. S5 A, available at http://www.jcb.org/cgi/content/full/jcb.200706196/DC1), whereas KIND domains do not detectably bind microtubules (Fig. S5 B). We confirmed that Capu-FH1FH2 cross-links microtubules by examining solutions of taxol-stabilized microtubules mixed with Capu-FH1FH2 by fluorescence microscopy and by performing polymerization assays under conditions that require a factor that stabilizes or cross-links tubulin nuclei
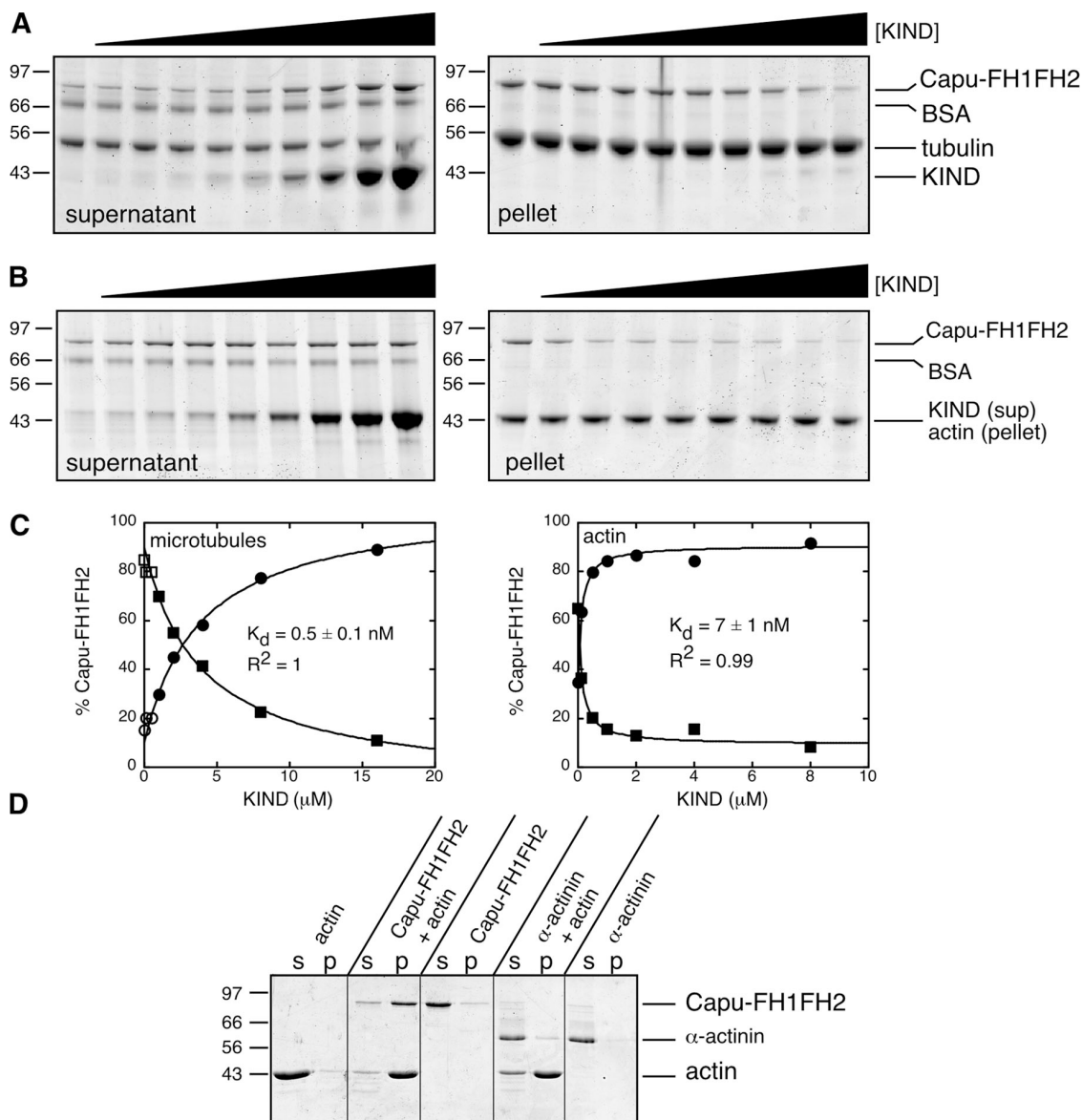
Figure 6. **The KIND domain, microtubules, and actin bind Capu-FH1FH2 competitively.** (A) Gels of cosedimentation assays show that the majority of the Capu-FH1FH2 cosediments when 0.5 μM Capu-FH1FH2 and 2 μM of stabilized microtubules are combined and centrifuged (left-most lanes of each gel). The addition of increasing amounts of KIND (0.0625, 0.125, 0.25, …16 μM) leads to the dissociation of Capu-FH1FH2 from microtubules, resulting in decreasing amounts of the formin in the pellet. (B) Gels of cosedimentation assays show that the majority of the Capu-FH1FH2 cosediments when 0.5 μM Capu-FH1FH2 and 2 μM of stabilized actin filaments are combined and centrifuged (left-most lanes of each gel). The addition of increasing amounts of KIND (0.0625, 0.125, 0.25, …16 μM) leads to the dissociation of Capu-FH1FH2 from actin, resulting in decreasing amounts of formin in the pellet. (C) Gels were quantified with Sypro-Red staining. Circles are Capu-FH1FH2 in the supernatant; squares are from the pellet. It takes ∼2.5 μM KIND to compete about half of the Capu-FH1FH2 away from microtubules because Capu-FH1FH2–microtubule interaction is very high affinity, as determined by fitting the data to a competition equation ($K_d = 0.5 \pm 0.1$ nM). Only ∼0.5 μM KIND is required to compete about half of the Capu-FH1FH2 away for actin, indicating that the affinity of Capu-FH1FH2 for actin is lower than that for microtubules, although still tight ($K_d = 7 \pm 1$ nM). Only the data that meet the assumptions (solid symbols) were used for the fit (see Materials and methods). (D) Actin cross-linking assay. 2 μM of filamentous actin plus 0.5 μM Capu-FH1FH2 or α-actinin were centrifuged at 16,000 g for 5 min. The supernatants and pellets were separated and analyzed by SDS-PAGE. Lines are for ease of comparison. The samples were all run on the same gel. Actin is found in the pellet in the presence of Capu-FH1FH2 and α-actinin, a known actin cross-linker.

(Fig. S5, E and F; Westermann et al., 2005). The addition of KIND to Capu and microtubules decreased microtubule binding by Capu in a dose-dependent manner (Fig. 6 A). About 2.5 μM KIND is necessary to compete half of the Capu-FH1FH2 away from 2 μM of polymerized tubulin, indicating that microtubules and KIND bind Capu-FH1FH2 with similar affinity. By fitting the data to a competition binding curve, we measured an affinity of Capu for microtubules of <1 nM (Fig. 6 C). We found no

difference in competition with NTSpir versus KIND alone, indicating that the WH2 cluster does not contribute measurably to this inhibitory interaction (Fig. S5 C).

Spir-KIND also regulates actin bundling by Capu (Fig. 6). In addition to binding barbed ends, some formins also bind the sides of actin filaments and bundle them (Harris et al., 2004; Michelot et al., 2005). To test for actin bundling, we mixed 0.5 μM Capu-FH1FH2 with 2 μM phalloidin-stabilized actin.

We observed bundles directly by fluorescence microscopy (Fig. S5 G) and indirectly with a low speed pelleting assay, in which only cross-linked networks or bundles of actin sediment (Fig. 6 D; Harris et al., 2006). The majority of the actin was bundled in the low speed pelleting assay. As a control, we used 0.5 μM α-actinin, a known actin cross-linker. Actin is in the supernatant when alone and in the pellet when α-actinin is added. Examination of the actin showed tight bundling in the presence of Capu-FH1FH2 similar to other formins and distinct from the loose networks created by α-actinin (Fig. S5 G; Wachsstock et al., 1993; Harris et al., 2006). Capu-FH1FH2 bundles more effectively than α-actinin, most likely reflecting a difference in off rates. We measured the effect of Spir on actin bundling by mixing 0.5 μM Capu-FH1FH2 with 2 μM actin and a range of concentrations of KIND or NTSpir. We then performed high speed cosedimentation assays and low speed cross-linking assays. We quantified Capu-FH1FH2 in the supernatants and pellets as a function of KIND concentration. By fitting the data to a competition binding curve, we found that the K_d of Capu for the sides of actin filaments is 7 ± 1 nM (high speed) or 6 ± 2 nM (low speed; Fig. 6, B and C; and not depicted).

Discussion

The *spire* and *cappuccino* genes have been linked since their discovery in a genetic screen 17 yr ago. We find that the KIND domain of Spir binds with high affinity to the Capu-FH2 domain at a stoichiometry of 2:2 (two KIND monomers to one FH2 dimer). We also find that the WH2 cluster of Spir interacts with Capu-FH2 but that this interaction is three orders of magnitude weaker than that between the Capu-FH2 and the KIND domain. Although we detect binding between the two domains, the Capu-FH2 domain has no direct effect on actin nucleation by the Spir-WH2 cluster. However, if the KIND domain is present and correctly folded, binding of the FH2 dimer increased nucleation activity of the WH2 cluster. On the other hand, the KIND domain potently inhibits actin nucleation by the Capu-FH2 domain. Constructs containing both the KIND and WH2 cluster do not enhance the inhibition of Capu-FH2–mediated actin nucleation or microtubule bundling over that observed for the KIND domain alone. For these reasons, we propose that the KIND–FH2 interaction is more physiologically relevant than the WH2–FH2 interaction. Additional structural and functional studies of the KIND domain are required to determine how many KIND domains are required to inhibit actin nucleation and to compete for actin and microtubule binding.

We originally identified the KIND module as a conserved region in the N-terminal half of Spir proteins (Ciccarelli et al., 2003) and named the region based on its sequence similarity to the C-lobe of the protein kinase fold (Ciccarelli et al., 2003). The KIND domain is found only in metazoa, and its consensus sequence lacks catalytic residues required for kinase activity. Because the substrates of protein kinases interact with α-helical regions in the C-lobe (Knighton et al., 1991; Tanoue and Nishida, 2002) we hypothesized that the KIND domain evolved from a functional kinase into a protein–protein interaction domain. The discovery that the Spir KIND domains bind specifically to Capu family FH2 domains supports this hypothesis.

What role do Spir and Capu play in oogenesis? Spir disappears from the oocyte cortex at stage 10, when rapid streaming normally begins and its absence in *spire* mutant flies leads to premature streaming. This strongly suggests that Spir plays an inhibitory role in rapid streaming. We do not yet know whether endogenous Capu has the same restricted temporal pattern observed for Spir. This information will be essential to understanding the nature of the Spir–Capu complex and its role during oogenesis. We find that Spir and Capu interact in the oocyte, and Rosales-Nieves et al. (2006) found that GFP fusions of these protein both exist at the oocyte cortex, placing them in an ideal location to coordinate actin and possibly anchor microtubules. Rapid streaming is, in part, characterized by bundling and movement of microtubules. Capu bundles microtubules, which is an activity regulated by Spir. If Spir is removed at stage 10 but Capu remains, Capu could play a role in reorganizing the microtubule cytoskeleton and possibly coordinating it with the actin cytoskeleton. A complete understanding of how Spir and Capu achieve this coordination depends on knowing when and how the Spir–Capu complex is regulated.

Capu and other members of the formin family nucleate de novo actin filament assembly and remain associated with elongating barbed ends of newly formed filaments (Pring et al., 2003; Quinlan et al., 2005). The activity of most formin family proteins is regulated by an autoinhibitory interaction between an N-terminal sequence (the Diaphanous inhibitory domain [DID]) and a C-terminal sequence (the Diaphanous autoinhibitory domain [DAD]). Small G proteins of the Rho family stimulate nucleation activity by binding to the DID domain and disrupting its interaction with DAD. However, Capu family formins lack both DID and DAD domains (Higgs and Peterson, 2005). In fact, Rosales-Nieves et al. (2006) did not observe autoinhibition when combining the N terminus of Capu with the FH2 domain, as has been observed for mDia1 (Li and Higgs, 2003). Our results argue strongly that Capu activity is regulated in trans by interaction with Spir.

The mechanism of actin nucleation by Spir is very different from that of formins like Capu. Spir binds four actin monomers using four closely apposed binding sites and then assembles them into a filament nucleus. After nucleation, Spir proteins remain associated with the slow-growing pointed end of the new filament. If Spir and Capu always function together as a single filament-forming complex, we suggest that their activities might synergize. One intriguing possibility is that Spir nucleates filaments whose free barbed ends are then handed off to Capu. Such a mechanism would enable the independent control of filament nucleation and barbed end binding. The tight binding that we measure suggests that Spir and Capu may not dissociate upon nucleation but that actin and microtubules do bind competitively. This idea begs two important questions: (1) Does the activation of Capu require the complete dissociation of Spir, or can the two proteins function together as a single filament–forming unit? (2) How is the Spir–Capu interaction modulated by upstream signaling systems? Recent data implicate the GTPase Rho as a regulator of Spir–Capu interaction in *Drosophila* (Rosales-Nieves et al., 2006). The Spir–Capu interaction is evolutionarily conserved, but whether or not this mode of regulation is conserved remains to be tested.

Materials and methods

Fly strains and immunofluorescence

Both Canton-S and w^{iso} flies were used as wild type (provided by R. Bainton, University of California, San Fransisco, San Fransisco, CA). $spir^1,cn^1,bn^1/Cyo,I(2)DTS513^1$ and $b^1,pr^1,spir^{2F},cn^1/CyO$ flies were obtained from T. Schupbach (Bloomington *Drosophila* Stock Center, Indiana University, Bloomington, IN). Transgenes were cloned into a pUASp vector and expressed in the germline with VP16nos:Gal4 or pCog:Gal4; NGT40:Gal4; VP16nos: Gal4 triple maternal driver lines (provided by L. Cooley, Yale, New Haven, CT). For immunofluorescence, they were fixed and stained according to methods described by Robinson and Cooley (1997). For actin visualization, ovaries were incubated in 1–2 U rhodamine-conjugated phalloidin (Invitrogen). For Spir immunolocalization, ovaries were incubated with ∼1 μg/ml antibody, and AlexaFluor488-conjugated goat anti–rabbit secondary antibody (Invitrogen) was used at a 1:1,000 dilution. Samples were mounted in fluorescence mounting medium (DakoCytomation). For live imaging, ovaries were dissected and teased apart under Halocarbon 700 oil (Sigma-Aldrich) at room temperature. In both cases, images were collected with a plan-Neofluor 25× 0.8 NA objective lens on a confocal microscope (LSM 510 META; Carl Zeiss MicroImaging, Inc.) with its proprietary software. Final rotations, cropping, and conversion to TIF format were performed in ImageJ (National Institutes of Health).

DNA constructs

Standard PCR and cloning methods were used to make DNA constructs.

Cell culture and transfections

NIH 3T3 mouse fibroblasts were cultured in DME supplemented with 10% FCS, glutamate, penicillin, and streptomycin at 37°C in a CO_2 (10%) incubator. The cells were transiently transfected with eukaryotic expression vectors with LipofectAMINE (Invitrogen). Immunofluorescence was performed as described previously (Otto et al., 2000). Cells were assayed 36 h after transfection. 5 μg/ml myc 9E10 mouse monoclonal antibodies (Santa Cruz Biotechnology, Inc.) and anti-TRITC–conjugated donkey anti–mouse (1:200; Dianova) were used. Fixed samples were mounted in a solution of 15 g Moviol, 60 ml PBS, 30 ml glycerol, and 2.25 g *N*-propyl-gallate. Images were collected with a 100× NA 1.3 oil U-V-I objective lens (Leica) on a fluorescence microscope (DMIRBE; Leica). Recordings were made with a camera (C4742-95; Hamamatsu) using Openlab 4.0.4 software (Improvision). Images were contrast enhanced and saved as TIF files using Openlab. All work was performed at room temperature.

Protein expression and purification

His-tagged proteins pQE-80L-m-Fmn2-FH2 (Fmn2-FH2), pQE-80L-hu-Spir1-KIND (Spir-1–KIND), pET-20b⁺-p150-Spir-KIND (KIND), and pET-20b⁺-p150-NTSpir (NTSpir) were expressed in *Escherichia coli* BL-21(DE3)pLysS cells. Cells were grown at 37°C to an optical density (A_{600}) of 0.6–0.8, induced with 0.25 mM IPTG, and harvested 3 h later. pET-20b⁺-p150-Spir-WH2 (WH2) and pET-20b⁺-p150-Spir-KCK-WH2(C459S) (KCK-WH2) were harvested after only 1.5 h. pET-20b⁺-Capu-FH2 (Capu-FH2) and pET-20b⁺-Capu-FH1FH2 (Capu-FH1FH2) were expressed in *E. coli* Rosetta bacteria (Novagen). Cells were grown at 37°C to an optical density (A_{600}) of 0.4–0.6, cooled to 21°C, induced with 0.1 mM IPTG, and grown overnight. His-tagged proteins were purified with BD Talon resin (CLONTECH Laboratories, Inc.), and most were further purified by anion exchange (monoQ) chromatography. See Table I for a summary of constructs and their extinction coefficients.

GST-tagged protein *E. coli* Rosetta bacteria was transformed with GST fusion protein expression vectors (GST-Spir1-KIND and GST-VKIND-KIND). Cells were grown at 37°C to an optical density (A_{600}) of 0.6–0.8, induced with 0.1 mM IPTG, and incubated at 21°C overnight. After centrifugation, the bacteria were suspended in TBS-Tween buffer (150 mM NaCl, 10 mM Tris-HCl, pH 7.4, and 0.1% Tween) and sonicated. The soluble extract was incubated with glutathione–Sepharose 4B beads (GE Healthcare) for 2 h at 4°C. The beads were washed twice with TBS-Tween buffer and resuspended in the same buffer for pull-down assays.

Immunoprecipitation

Immunoprecipitation from fly ovary was performed according to the methods of Rosales-Nieves et al. (2006; ∼100 flies were used for each condition). Immunoprecipitation from tissue culture cells was performed as follows: 36 h after transfection, NIH 3T3 cells were lysed with immunoprecipitation lysis buffer (25 mM Tris-HCl, pH 7.5, 150 mM NaCl, 2 mM EDTA, 2 mM EGTA, 10% glycerol, 0.1% NP-40, 2 μg/ml leupeptin, 2 μg/ml aprotinin,

1 mM PMSF, 10 mM NaF, and 0.2 mM Na_3VO_4). Anti–myc 9E10 monoclonal antibodies (Santa Cruz Biotechnology, Inc.) were added to the cleared cell lysate to a final concentration of 5 μg/ml and incubated for 1 h on ice. Protein G–agarose (Roche) was added, and the sample was rotated for 150 min at 4°C. The beads were washed twice with immunoprecipitation lysis buffer, and bound proteins were analyzed by Western blotting.

GST pull-down experiments were performed as follows: 1–2 μg GST/GST-VKIND-KIND/GST-hu-Spir-1-KIND/GST-hu-Spir-1-KIND-WH2 fusion protein was coupled to 50 μl glutathione–Sepharose beads and washed twice with pull-down buffer (25 mM Tris-HCl, pH 7.4, 150 mM NaCl, 1 mM EDTA, 0.1% NP-40, and 10% glycerol). NIH 3T3 fibroblasts transiently expressing EGFP-mDia1-F2 and EGFP-m-Fmn2-FH2 were lysed with pull-down buffer for 40 min at 4°C. Cleared lysate was incubated with the glutathione–Sepharose beads for 2 h. The beads were gently washed five times in pull-down buffer and boiled in SDS sample buffer. The samples were analyzed by Western blotting.

Protein labeling

Acanthamoeba actin was labeled with pyrene iodoacetamide as described previously (Cooper et al., 1983). Purified KIND (human and *Drosophila*) was incubated with a 1–2.5-fold molar excess of AlexaFluor488-maleimide (Invitrogen) in labeling buffer (50 mM KCl, 50 μM Tris(2-carboxyethyl) phosphine [TCEP], and 10 mM Hepes, pH 7) for 30 min at 24°C. The reaction was quenched by the addition of 10 mM DTT. Free dye was removed by gel filtration and verified by SDS-PAGE. Protein concentration was determined by absorbance at 280 nm using molar extinction coefficients (human, 22,620 cm⁻¹; *Drosophila*, 17,452 cm⁻¹; Table I) and correcting for dye absorbance ($0.11*A_{496}$). The concentration of incorporated dye was determined by absorbance at 496 nm using an extinction coefficient of 71,000 cm⁻¹. The labeling efficiency of Spir-1–KIND varied from 85 to 94% at all dye/protein ratios above 1:1, suggesting that Spir-1–KIND contains a single accessible and reactive cysteine. The labeling efficiency of KIND was >100% at dye/protein ratios above 1:1. Therefore, we underlabeled KIND (15–45%) to increase the probability of only labeling one cysteine per protein.

To label Capu-FH1FH2, we added a Lys-Cys-Lys to the C terminus. To label the WH2 cluster, we first mutated the only native cysteine in WH2 to serine and then engineered a Lys-Cys-Lys sequence onto the N terminus of the polypeptide. Mutation and labeling had no effect on the actin nucleation activity of either construct. We followed the labeling protocol used for the KIND domains except that the labeling conditions were between one- and twofold molar excess of AlexaFluor488-maleimide for 5–10 min at 24°C. Both proteins were labeled ∼100%.

Analytical ultracentrifugation

Extinction coefficients for Spir-1–KIND and Fmn2-FH2 were determined by spinning purified, recombinant proteins at 40,000 rpm in an analytical ultracentrifuge (XL-I; Beckman Coulter). Proteins and buffer blanks were loaded into two-channel centrepieces and spun until the meniscus was depleted of protein. We then measured the relative index of refraction and the absorbance at 280 nm as a function of radius. We determined protein concentration from the index of refraction (assuming 3.3 mg/ml/fringe displacement) and compared it with absorbance at 280 nm (assuming an optical path length of 1.2 cm).

Table I. **Summary of purified proteins used in biochemical assays (all His tagged)**

Construct name	Residues	Extinction coefficient
Drosophila isoforms		
NTSpir	1–520	25,575ᵃ cm⁻¹
KIND	1–327	17,452ᵃ,ᵇ cm⁻¹
WH2	366–482	15,220ᵇ cm⁻¹
Capu-FH2	573–1,058	53,760ᵃ cm⁻¹
Capu-FH1FH2	467–1,058	75,200ᵃ cm⁻¹
Mammalian isoforms		
Spir-1–KIND	2–271	22,620ᶜ cm⁻¹
Fmn2-FH2	1,124–1,567	25,445ᶜ cm⁻¹

ᵃQuantitative SDS-PAGE with Sypro-Red staining.
ᵇComparison of absorbance at 280 nM of native protein with protein denatured in 6 M GnHCl.
ᶜAnalytical ultracentrifugation.

Solution molecular weights were determined by spinning samples to equilibrium in an analytical ultracentrifuge (XL-I; Beckman Coulter) and measuring protein concentration as a function of radius. For individual protein, we used three different concentrations ($\sim$0.5, 0.25, and 0.125 mg/ml). For KIND and Capu-FH1FH2 together, we used three molar ratios of AlexaFluor488-labeled Capu-FH1FH2 and KIND (1 [Capu dimer]:1 [KIND], 1:2, and 1:4). We spun samples to equilibrium at three speeds and measured protein concentration as a function of radius by absorbance at 280 or 500 nm to track the fluorophore. We then globally fit all of the sedimentation curves obtained at different concentrations and speeds (nine datasets) to different models (Johnson et al., 1981) using Winnonln (J. Lary and D. Yphantis, National Analytical Ultracentrifugation Facility, Storrs, CT) or Ultrascan (B. Demeler, University of Texas Health Science Center, San Antonio, TX).

Pyrene actin assembly assays

We performed pyrene actin assembly assays as described previously (Zalevsky et al., 2001). In brief, we used 4 µM *Acanthamoeba* actin doped with 5% pyrene-labeled actin. Ca^{2+}-actin was converted to Mg^{2+}-actin before each reaction by a 2-min incubation with 50 µM $MgCl_2$ and 200 µM EGTA. All components except actin were combined before the initiation of polymerization. All polymerization reactions contained 50 mM KCl, 1 mM $MgSO_4$, 1 mM EGTA, and 10 mM imidazole, pH 7.0. Pyrene fluorescence was measured by a multifrequency fluorometer (K2; ISS), and data were analyzed using KaleidaGraph (Synergy Software) and in-house software.

Polarization anisotropy

Low concentrations (10–20 nM) of the protein labeled with AlexaFluor488 (Spir-1–KIND, KIND, or WH2) was mixed with unlabeled target protein (Fmn2-FH2, Capu-FH1FH2, or Capu-FH2) at the indicated concentrations in KMEH (50 mM KCl, 20 mM Hepes, pH 7.0, 1 mM $MgCl_2$, 1 mM EGTA, and 1 mM TCEP), and polarization anisotropy was measured at 24°C using a multifrequency fluorometer (K2; ISS) and analyzed using KaleidaGraph (Synergy Software). Under the conditions used in our study, anisotropy is a measure of the rotational mobility of the labeled protein. We excited the fluorophore with plane polarized light at 488 nm (with a 488-nm bandpass filter) and measured emission at 520 nm (KV500 and KV520 filters) at polarizations both parallel ($I_{||}$) and perpendicular ($I_\perp$) to the excitation light. We simultaneously monitored total intensity to ensure that the quantum efficiency of the fluorophore was independent of the protein complex. In the case of labeled WH2, the intensity changed in a concentration-dependent saturable manner, so we used this value instead of anisotropy. We determined equilibrium dissociation constants using a quadratic binding model as previously described (Zalevsky et al., 2001).

In competition binding experiments, we determined the dissociation constant of the unlabeled protein by fitting anisotropy data to the function (Vinson et al., 1998)

$$r = r_f + \frac{(r_b - r_f)}{K_d \dfrac{[C] + K_{d2}}{K_{d2}[R_o]} + 1}$$

where K_{d2} is the dissociation constant of the nonfluorescent competitor, [C] is the total concentration of the competitor, and $[R_o]$ is the concentration of free Capu-FH1FH2 when [C] = 0. For this analysis, $[R_o]$ and K_d are determined from the anisotropy in the absence of competitor, and K_{d2} is determined from fitting the above equation to experimental data. This function is an approximation and is only valid when unlabeled KIND and formin are in excess over the labeled protein. These conditions were met in our competition binding experiments.

Microtubule-binding assay

Purified porcine brain tubulin was provided by A. Carter (laboratory of R. Vale, University of California, San Fransisco, San Fransisco, CA). Microtubules were stabilized with taxol, and all experiments were performed in KMEH. Capu-FH1FH1, Fmn2-FH2, KIND, and Spir-1–KIND were cleared by centrifugation at 100,000 g for 20 min at 24° C before each assay. Microtubules were added at four- to eightfold molar excess. Samples were incubated for 15 min and centrifuged at 100,000 g for 10 min at 24°C. Supernatants were removed, and pellets were washed before resuspending. Both supernatants and pellets were analyzed by SDS-PAGE.

In competition experiments, KIND or NTSpir was added in a twofold concentration series ranging from 16 to 0.0625 µM (i.e., 16, 8, 4, …0.0625 µM), and 20 µg/ml BSA was added as a loading standard.

These gels were stained with Sypro-Red (Invitrogen) and quantified using a multiformat imager (Typhoon 9400; GE Healthcare) and ImageQuant software (GE Healthcare). We determined the dissociation constant of the unlabeled protein by fitting binding data to the equation above. In this case, K_{d2} is the dissociation constant of the competitor (KIND or NTSpir) for Capu-FH1FH2, [C] is the concentration of the competitor, and $[R_o]$ is the concentration of free Capu-FH1FH2 when [C] = 0. For this analysis, K_{d2} was determined by fluorescence anisotropy (5 nM), and K_d, the dissociation constant of Capu-FH1FH2 for microtubules, is determined by fitting the above equation to experimental data. This function is an approximation and is only valid when the competitor and microtubules are in excess over Capu-FH1FH2. Only the data points that met these conditions were fit.

Cross-linking assays

Two actin-binding assays were used. An actin cross-linking assay was performed according to Harris et al. (2006) with minor modifications. 50-µl solutions containing 2 µM phalloidin-stabilized actin plus 0.5 µM Capu-FH1FH2 or α-actinin or each component separately were mixed in KMEH, allowed to stand at RT for 10 min, and centrifuged at 16,000 g for 5 min. 40 µl of the supernatant was removed, and the pellet was washed once and resuspended in 50 µl. Equal amounts of supernatants and pellets were analyzed by SDS-PAGE. For microscopy experiments, we substituted AlexaFluor488-phalloidin for unlabeled phalloidin. After standing for at least 10 min, solutions were diluted 1:100 in KMEH and added to poly-L-lysine–coated flow chambers at room temperature. Images were collected with a plan Apo 60× 1.2 NA objective lens and camera (C4742-98; Hamamatsu) on a microscope (TE300; Nikon) with Simple PCI software (Compix, Inc.).

Two microtubule cross-linking assays were used. The first assay was performed according to the methods of Westermann et al. (2005). 50-µl solutions containing 10 µM tubulin (doped with 10% rhodamine-tubulin [Cytoskeleton, Inc.]) plus 0.5 µM Capu-FH1FH2 or GST-Spastin(E542A) (a mutant in the Walker B site that does not sever [Roll-Mecak and Vale, 2005]) were mixed on ice in 80 mM Pipes, pH 6.9, 1 mM EGTA, 1 mM $MgCl_2$, 1 mM GTP, and 25% glycerol. They were incubated at 37°C for 25 min and fixed with 1% gluteraldehyde. Samples were diluted 1:100, introduced into a flow chamber, and examined by fluorescence microscopy. For the second assay, the microtubules were prepolymerized at high concentration (18 µM), taxol stablized, and diluted and combined with Capu-FH1FH2 or GST-Spastin(E542A) (10:0.5 µM). These solutions were allowed to stand at room temperature for at least 15 min before dilution (1:100) and visualization in a flow chamber, with the same equipment used for actin cross-linking assays.

Online supplemental material

Fig. S1 shows a stage 9 egg chamber expressing Spir-mRFP (A), immunofluorescence and Western blots showing the specificity of anit-Spir antibody (B–D), complete Western blots from Fig. 1 E (E), and a Western blot of an oocyte coimmunoprecipitated with and without latrunculin (F). Fig. S2 shows additional images of Spir and Capu expression in NIH 3T3 cells (A–D), GST pull-down with mammalian isoforms of Spir and Capu (E), an anisotropy experiment with Capu-FH2 (F), and an anisotropy experiment with mammalian isoforms of Spir and Capu (G). Fig. S3 shows the inhibition of Capu-FH2–mediated actin nucleation by KIND (A–C), sample analysis of polymerization assays (D), the inhibition curve for mammalian isoforms of Spir and Capu (E), and alternate inhibition analysis (F). Fig. S4 shows that KIND does not influence spontaneous actin polymerization (A and B) and that Spir-1–KIND does not interact with mDia1 or mDia2 (C). Fig. S5 shows gels of FH2 domains and KIND mixed with tubulin (A and B), a cosedimentation assay with Capu-FH1FH2, tubulin, and NTSpir (instead of KIND; C and D), and images of Capu-FH1FH2–mediated tubulin polymerization and bundling of microtubules and actin (E–G). Online supplemental material is available at http://www.jcb.org/cgi/content/full/jcb.200706196/DC1.

References

Ciccarelli, F.D., P. Bork, and E. Kerkhoff. 2003. The KIND module: a putative signalling domain evolved from the C lobe of the protein kinase fold. *Trends Biochem. Sci.* 28:349–352.

Clark, I., E. Giniger, H. Ruohola-Baker, L.Y. Jan, and Y.N. Jan. 1994. Transient posterior localization of a kinesin fusion protein reflects anteroposterior polarity of the *Drosophila* oocyte. *Curr. Biol.* 4:289–300.

Cooper, J.A., S.B. Walker, and T.D. Pollard. 1983. Pyrene actin: documentation of the validity of a sensitive assay for actin polymerization. *J. Muscle Res. Cell Motil.* 4:253–262.

Emmons, S., H. Phan, J. Calley, W. Chen, B. James, and L. Manseau. 1995. Cappuccino, a *Drosophila* maternal effect gene required for polarity of the egg and embryo, is related to the vertebrate limb deformity locus. *Genes Dev.* 9:2482–2494.

Harris, E.S., F. Li, and H.N. Higgs. 2004. The mouse formin, FRLalpha, slows actin filament barbed end elongation, competes with capping protein, accelerates polymerization from monomers, and severs filaments. *J. Biol. Chem.* 279:20076–20087.

Harris, E.S., I. Rouiller, D. Hanein, and H.N. Higgs. 2006. Mechanistic differences in actin bundling activity of two mammalian formins, FRL1 and mDia2. *J. Biol. Chem.* 281:14383–14392.

Higgs, H.N., and K.J. Peterson. 2005. Phylogenetic analysis of the formin homology 2 domain. *Mol. Biol. Cell.* 16:1–13.

Johnson, M.L., J.J. Correia, D.A. Yphantis, and H.R. Halvorson. 1981. Analysis of data from the analytical ultracentrifuge by nonlinear least-squares techniques. *Biophys. J.* 36:575–588.

Kerkhoff, E., J.C. Simpson, C.B. Leberfinger, I.M. Otto, T. Doerks, P. Bork, U.R. Rapp, T. Raabe, and R. Pepperkok. 2001. The Spir actin organizers are involved in vesicle transport processes. *Curr. Biol.* 11:1963–1968.

Knighton, D.R., J.H. Zheng, L.F. Ten Eyck, V.A. Ashford, N.H. Xuong, S.S. Taylor, and J.M. Sowadski. 1991. Crystal structure of the catalytic subunit of cyclic adenosine monophosphate-dependent protein kinase. *Science.* 253:407–414.

Kobielak, A., H.A. Pasolli, and E. Fuchs. 2004. Mammalian formin-1 participates in adherens junctions and polymerization of linear actin cables. *Nat. Cell Biol.* 6:21–30.

Le Goff, C., V. Laurent, K. Le Bon, G. Tanguy, A. Couturier, X. Le Goff, and R. Le Guellec. 2006. pEg6, a SPIR family member, is a maternal gene encoding a vegetally localised mRNA in *Xenopus* embryos. *Biol. Cell.* 98:697–708.

Leader, B., and P. Leder. 2000. Formin-2, a novel formin homology protein of the cappuccino subfamily, is highly expressed in the developing and adult central nervous system. *Mech. Dev.* 93:221–231.

Leader, B., H. Lim, M.J. Carabatsos, A. Harrington, J. Ecsedy, D. Pellman, R. Maas, and P. Leder. 2002. Formin-2, polyploidy, hypofertility and positioning of the meiotic spindle in mouse oocytes. *Nat. Cell Biol.* 4:921–928.

Li, F., and H.N. Higgs. 2003. The mouse Formin mDia1 is a potent actin nucleation factor regulated by autoinhibition. *Curr. Biol.* 13:1335–1340.

Manseau, L.J., and T. Schupbach. 1989. cappuccino and spire: two unique maternal-effect loci required for both the anteroposterior and dorsoventral patterns of the *Drosophila* embryo. *Genes Dev.* 3:1437–1452.

Manseau, L., J. Calley, and H. Phan. 1996. Profilin is required for posterior patterning of the *Drosophila* oocyte. *Development.* 122:2109–2116.

Mees, A., R. Rock, F.D. Ciccarelli, C.B. Leberfinger, J.M. Borawski, P. Bork, S. Wiese, M. Gessler, and E. Kerkhoff. 2005. Very-KIND is a novel nervous system specific guanine nucleotide exchange factor for Ras GTPases. *Gene Expr. Patterns.* 6:79–85.

Michelot, A., C. Guerin, S. Huang, M. Ingouff, S. Richard, N. Rodiuc, C.J. Staiger, and L. Blanchoin. 2005. The formin homology 1 domain modulates the actin nucleation and bundling activity of *Arabidopsis* FORMIN1. *Plant Cell.* 17:2296–2313.

Otto, I.M., T. Raabe, U.E. Rennefahrt, P. Bork, U.R. Rapp, and E. Kerkhoff. 2000. The p150-Spir protein provides a link between c-Jun N-terminal kinase function and actin reorganization. *Curr. Biol.* 10:345–348.

Pokrywka, N.J., and E.C. Stephenson. 1995. Microtubules are a general component of mRNA localization systems in *Drosophila* oocytes. *Dev. Biol.* 167:363–370.

Polesello, C., I. Delon, P. Valenti, P. Ferrer, and F. Payre. 2002. Dmoesin controls actin-based cell shape and polarity during *Drosophila melanogaster* oogenesis. *Nat. Cell Biol.* 4:782–789.

Pring, M., M. Evangelista, C. Boone, C. Yang, and S.H. Zigmond. 2003. Mechanism of formin-induced nucleation of actin filaments. *Biochemistry.* 42:486–496.

Quinlan, M.E., J.E. Heuser, E. Kerkhoff, and R.D. Mullins. 2005. *Drosophila* Spire is an actin nucleation factor. *Nature.* 433:382–388.

Robinson, D.N., and L. Cooley. 1997. Examination of the function of two kelch proteins generated by stop codon suppression. *Development.* 124:1405–1417.

Roll-Mecak, A., and R.D. Vale. 2005. The *Drosophila* homologue of the hereditary spastic paraplegia protein, spastin, severs and disassembles microtubules. *Curr. Biol.* 15:650–655.

Rosales-Nieves, A.E., J.E. Johndrow, L.C. Keller, C.R. Magie, D.M. Pinto-Santini, and S.M. Parkhurst. 2006. Coordination of microtubule and microfilament dynamics by *Drosophila* Rho1, Spire and Cappuccino. *Nat. Cell Biol.* 8:367–376.

Schaber, M.D., M.B. O'Hara, V.M. Garsky, S.C. Mosser, J.D. Bergstrom, S.L. Moores, M.S. Marshall, P.A. Friedman, R.A. Dixon, and J.B. Gibbs. 1990. Polyisoprenylation of Ras in vitro by a farnesyl-protein transferase. *J. Biol. Chem.* 265:14701–14704.

Schumacher, N., J.M. Borawski, C.B. Leberfinger, M. Gessler, and E. Kerkhoff. 2004. Overlapping expression pattern of the actin organizers Spir-1 and formin-2 in the developing mouse nervous system and the adult brain. *Gene Expr. Patterns.* 4:249–255.

Serbus, L.R., B.J. Cha, W.E. Theurkauf, and W.M. Saxton. 2005. Dynein and the actin cytoskeleton control kinesin-driven cytoplasmic streaming in *Drosophila* oocytes. *Development.* 132:3743–3752.

Tanoue, T., and E. Nishida. 2002. Docking interactions in the mitogen-activated protein kinase cascades. *Pharmacol. Ther.* 93:193–202.

Theurkauf, W.E. 1994. Premature microtubule-dependent cytoplasmic streaming in cappuccino and spire mutant oocytes. *Science.* 265:2093–2096.

Theurkauf, W.E., S. Smiley, M.L. Wong, and B.M. Alberts. 1992. Reorganization of the cytoskeleton during *Drosophila* oogenesis: implications for axis specification and intercellular transport. *Development.* 115:923–936.

Vinson, V.K., E.M. De La Cruz, H.N. Higgs, and T.D. Pollard. 1998. Interactions of *Acanthamoeba* profilin with actin and nucleotides bound to actin. *Biochemistry.* 37:10871–10880.

Wachsstock, D.H., W.H. Schwartz, and T.D. Pollard. 1993. Affinity of alpha-actinin for actin determines the structure and mechanical properties of actin filament gels. *Biophys. J.* 65:205–214.

Wallar, B.J., and A.S. Alberts. 2003. The formins: active scaffolds that remodel the cytoskeleton. *Trends Cell Biol.* 13:435–446.

Wellington, A., S. Emmons, B. James, J. Calley, M. Grover, P. Tolias, and L. Manseau. 1999. Spire contains actin binding domains and is related to ascidian posterior end mark-5. *Development.* 126:5267–5274.

Westermann, S., A. Avila-Sakar, H.W. Wang, H. Niederstrasser, J. Wong, D.G. Drubin, E. Nogales, and G. Barnes. 2005. Formation of a dynamic kinetochore-microtubule interface through assembly of the Dam1 ring complex. *Mol. Cell.* 17:277–290.

Xu, Y., J.B. Moseley, I. Sagot, F. Poy, D. Pellman, B.L. Goode, and M.J. Eck. 2004. Crystal structures of a Formin Homology-2 domain reveal a tethered dimer architecture. *Cell.* 116:711–723.

Zalevsky, J., I. Grigorova, and R.D. Mullins. 2001. Activation of the Arp2/3 complex by the *Listeria* acta protein. Acta binds two actin monomers and three subunits of the Arp2/3 complex. *J. Biol. Chem.* 276:3468–3475.